Performance of Ambient Backscatter Systems Using Reconfigurable Intelligent Surface

Yunfei Chen, *Senior Member, IEEE*

***Abstract*— Reconfigurable intelligent surface (RIS) has been proved effective in improving the performance of communications. In this letter, the effect of RIS on individual links in ambient backscatter communications is examined. The average bit error rate is derived for the cases when the source-to-reader (S-R) link, the source-to-tag (S-T) link, or both S-R and S-T links use RIS to enhance their links. Numerical results show that generally speaking the performance of ambient backscatter communications degrades when the number of RIS elements in the S-R link increases, while improves when the number of RIS elements in the S-T link increases, when RIS is used to enhance the relevant link. Also, the two effects cancel out but in general the performance improves when both links are enhanced by RIS.**

***Index Terms*— Ambient backscatter communications, performance analysis, reconfigurable intelligent surface.**

I. Introduction

Recently, ambient backscatter communication has been proposed [1] - [4]. A key performance measure of ambient backscatter communication is the bit error rate (BER). Hence, various signal detectors have been studied in terms of their BER. To name a few, in [5], coherent detectors and energy detectors were proposed for backscatter communications. In [6], the tag signal was encoded using Manchester coding and the corresponding maximum likelihood detector was then proposed. In [7], energy detectors were proposed for orthogonal-frequency-division-multiplexing signals. In [8], the physical layer security of ambient backscatter with hardware impairment was investigated. In [9], energy and maximum likelihood detectors were proposed and analyzed using Gaussian approximation. These works have provided useful guidance on ambient backscatter designs.

On the other hand, reconfigurable intelligent surface (RIS) has arisen as an effective way of improving wireless channels [10]. It uses a reflective surface that is able to adjust the phase continuously [11] or discretely [12], [13], as well as use amplitude control [14] to compensate the channel fading for diversity gain, and has been adopted in different communications systems for performance improvement, including ambient backscatter communications. In [15], an ambient backscatter communications system using RIS in all links was studied to show improvement over systems without RIS. In [16], RIS was deployed in a bi-static backscatter communications system and beamforming was performed to minimize transmission power. These works have provided insights on the use of RIS in ambient backscatter communications. However, they fail to reveal the impact of RIS on the individual links in ambient backscatter communications. It is observed from [5] - [9] that a good signal quality is not always beneficial for ambient backscatter communications.

In this letter, the effect of RIS on individual links in the ambient backscatter communications system is examined. The BERs using RIS in the source-to-reader (S-R) link, in the source-to-tag (S-T) link and in both links are analyzed. Integral expressions for the average BERs are derived using the large signal-to-noise ratio (SNR) and Gamma approximations. Numerical results are presented to show that the BER performance improves when the number of RIS elements in the S-T link increases but deteriorates when the number of RIS elements in the S-R link increases, in the general case. When both the S-T and S-R links use RIS, the BER performance still improves but the improvement is smaller. These are based on the assumption that RIS is used to enhance the links.

Yunfei Chen is with the School of Engineering, University of Warwick, Coventry, UK, CV4 7AL. (e-mail: Yunfei.Chen@warwick.ac.uk)

II. System Model

Fig. 1 shows the system considered. The ambient radio frequency (RF) source transmits the RF signal $s[n]$ assumed to be Gaussian with $s[n] \sim \mathcal{CN}(0, P_s)$ and unknown. When the tag transmits a bit of '0', it does not reflect the signal from source so that the tag reader only receives the direct signal as

$$y[n] = h_{sr}s[n] + w[n] \tag{1}$$

where $n = 1, 2, \cdots, N$ index the signals received, h_{sr} is the channel gain in the S-R link from the RF source to the tag reader with $h_{sr} \sim \mathcal{CN}(0, \sigma_{sr}^2)$ and $w[n]$ is the additive white Gaussian noise (AWGN) with $w[n] \sim \mathcal{CN}(0, \sigma_w^2)$. When the tag transmits a bit of '1', it reflects the signal from source so that the tag reader receives both the direct signal from the RF source and the reflected signal from the tag as

$$y[n] = h_{sr}s[n] + \alpha h_{st}h_{tr}s[n] + w[n] \tag{2}$$

where h_{st} is the channel gain in the S-T link from the RF source to the tag with $h_{st} \sim \mathcal{CN}(0, \sigma_{st}^2)$, h_{tr} is the channel gain in the link from the tag to the reader (T-R) with $h_{tr} \sim \mathcal{CN}(0, \sigma_{tr}^2)$ and α is the tag coefficient.

Denote $h_0 = h_{sr}$ and $h_1 = h_{sr} + \alpha h_{st}h_{tr}$. From (1) and (2), the maximum likelihood detector can be derived and its BER is [5]

$$\begin{aligned} P_e(\rho) &= \frac{\gamma(N, N\frac{\rho\ln\rho}{\rho-1}) + \Gamma(N, N\frac{\ln\rho}{\rho-1})}{2\Gamma(N)}, 0 < \rho < 1 \\ P_e(\rho) &= \frac{\Gamma(N, N\frac{\rho\ln\rho}{\rho-1}) + \gamma(N, N\frac{\ln\rho}{\rho-1})}{2\Gamma(N)}, \rho > 1 \end{aligned} \tag{3}$$

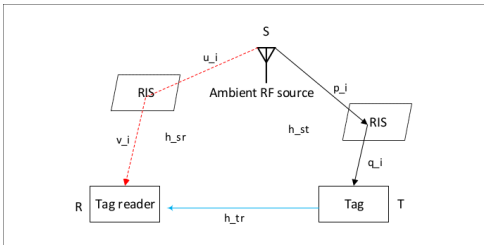

Fig. 1. The system considered.

where $\rho = \frac{|h_1|^2+\frac{\sigma_w^2}{P_s}}{|h_0|^2+\frac{\sigma_w^2}{P_s}}$, $\Gamma(\cdot)$ is the Gamma function [17, eq. (8.310.1)], $\gamma(\cdot,\cdot)$ is the lower Gamma function [17, eq. (8.350.1)] and $\Gamma(\cdot,\cdot)$ is the upper Gamma function [17, 8.350.2]. One sees from (3) that the BER is minimum when $\rho \to 0$ or $\rho \to \infty$ and maximum when $\rho \to 1$. To reduce BER, $|h_0|^2$ and $|h_1|^2$ must be as dissimilar as possible.

Using (3), the average BER is derived as

$$\bar{P}_e = \frac{1}{2\Gamma(N)}[\int_0^1 [\gamma(N, N\frac{\rho\ln\rho}{\rho-1}) + \Gamma(N, N\frac{\ln\rho}{\rho-1})]f(\rho)d\rho + \int_1^\infty [\Gamma(N, N\frac{\rho\ln\rho}{\rho-1}) + \gamma(N, N\frac{\ln\rho}{\rho-1})]f(\rho)d\rho] \quad (4)$$

where $f(\rho)$ is the probability density function (PDF) of ρ to be determined in the next section.

III. Derivation

Define $\gamma_s = \frac{P_s}{\sigma_w^2}$ as the SNR. As $\gamma_s \to \infty$, $\rho \approx \frac{|h_1|^2}{|h_0|^2}$. We will use this approximation to derive the PDF of ρ. Simulation reveals that it is accurate when γ_s is above 20 dB. The results in the general case are difficult to obtain.

A. Without RIS

For the original system without RIS, one has

$$\rho \approx |1 + \alpha\frac{h_{st}}{h_{sr}}h_{tr}|^2 = |1 + \frac{\alpha\sigma_{st}\sigma_{tr}}{\sigma_{sr}}\frac{h'_{st}}{h'_{sr}}h'_{tr}|^2 \quad (5)$$

where $h'_{st}, h'_{sr}, h'_{tr} \sim \mathcal{CN}(0,1)$. Denote the direct-to-reflection ratio (DRR) as $\beta_o = \frac{\sigma_{sr}^2}{\alpha^2\sigma_{st}^2\sigma_{tr}^2}$. Conditioned on h'_{st} and h'_{sr}, ρ is the square of a Rician random variable. Thus, the conditional PDF of ρ is derived as [18]

$$f(\rho|h'_{st}, h'_{sr}) = \beta_o\frac{|h'_{sr}|^2}{|h'_{st}|^2}e^{-(1+\rho)\beta_o\frac{|h'_{sr}|^2}{|h'_{st}|^2}}I_0\left(2\sqrt{\rho}\beta_o\frac{|h'_{sr}|^2}{|h'_{st}|^2}\right) \quad (6)$$

where $I_0(\cdot)$ is the zero-th order modified Bessel function of the first type [17, eq. (8.406.1)]. Also, since both h'_{st} and h'_{sr} are complex Gaussian, $X_o = \frac{|h'_{sr}|^2}{|h'_{st}|^2}$ is the ratio of two exponential random variables to give its PDF

$$f_{X_o}(x) = \frac{1}{(1+x)^2}, x > 0. \quad (7)$$

Thus, the PDF of ρ is

$$f(\rho) = \beta_o\int_0^\infty \frac{x}{(1+x)^2}e^{-(1+\rho)\beta_o x}I_0\left(2\sqrt{\rho}\beta_o x\right)dx. \quad (8)$$

This integral cannot be further simplified unless one uses the series expansion of the Bessel function but this will lead to an infinite series for truncation.

B. RIS in S-R Link

If the S-R link uses RIS, one has [11]

$$h_{sr} = \sum_{i=1}^I u_i e^{j\theta_i}v_i = \sum_{i=1}^I |u_i||v_i| \quad (9)$$

where I is the number of RIS elements, u_i is the channel from the source to i-th element of RIS with $u_i \sim \mathcal{CN}(0,\sigma_u^2)$, v_i is the channel from the i-th element of RIS to the tag reader with $v_i \sim \mathcal{CN}(0,\sigma_v^2)$, and θ_i is the adjustable phase shift with $\theta_i = -\angle u_i - \angle v_i$ to enhance the link. For analytical tractability, we consider continuous phase shift. Amplitude control is not used to save cost of power amplification. Using (9) in (5), one has

$$\rho \approx |1 + \frac{\alpha\sigma_{st}\sigma_{tr}}{\sigma_u\sigma_v}\frac{h'_{st}}{\sum_{i=1}^I |u'_i||v'_i|}h'_{tr}|^2 \quad (10)$$

where $u'_i, v'_i \sim \mathcal{CN}(0,1)$. The conditional PDF of ρ is

$$f(\rho|X_r) = \beta_r X_r e^{-(1+\rho)\beta_r X_r}I_0\left(2\sqrt{\rho}\beta_r X_r\right) \quad (11)$$

where $\beta_r = \frac{\sigma_u^2\sigma_v^2}{\alpha^2\sigma_{st}^2\sigma_{tr}^2}$ and $X_r = \frac{(\sum_{i=1}^I |u'_i||v'_i|)^2}{|h'_{st}|^2}$. The random variable $\sum_{i=1}^I |u'_i||v'_i|$ does not have any closed-form. Extensive simulation suggests that it can be well approximated by Gamma distribution. Using moment-matching, one has $E\{\sum_{i=1}^I |u'_i||v'_i|\} = \frac{\pi}{4}I = k*c$ and $E\{(\sum_{i=1}^I |u'_i||v'_i|)^2\} = I + I(I-1)\frac{\pi^2}{16} = k(k+1)*c^2$, where $k*c$ and $k(k+1)*c^2$ are the first- and second-order moments of Gamma distribution, k is the shape parameter and c is the scale parameter. Thus,

$$f_{\sum_{i=1}^I |u'_i||v'_i|}(r) = \frac{r^{k-1}}{\Gamma(k)c^k}e^{-\frac{r}{c}} \quad (12)$$

with $k = I\frac{\pi/4}{4/\pi-\pi/4}$ and $c = 4/\pi - \pi/4$ obtained by solving the two moment equations. The cumulative distribution function (CDF) of X_r can be derived as

$$\begin{aligned} F_{X_r}(x) &= 1 - Pr\{|h'_{st}|^2 < \frac{1}{x}(\sum_{i=1}^I |u'_i||v'_i|)^2\} \\ &= \int_0^\infty e^{-\frac{r^2}{x}}\frac{r^{k-1}}{\Gamma(k)c^k}e^{-\frac{r}{c}}dr \\ &= \left(\frac{x}{2c^2}\right)^{\frac{k}{2}}e^{\frac{x}{8c^2}}D_{-k}\left(\sqrt{\frac{x}{2c^2}}\right) \end{aligned} \quad (13)$$

where the second equation is obtained by using the exponential distribution of $|h'_{st}|^2$, the third equation is obtained by using [17, eq. (3.462.1)], and $D(\cdot)$ is the parabolic cylinder function [17, eq. (9.240)]. Finally, the unconditional PDF of ρ can be calculated by differentiating (13) with respect to x to get the PDF using [17, eq. (9.247.3)] and then with (11) as

$$f(\rho) = \frac{\beta_r}{(2c^2)^{\frac{k}{2}}}\int_0^\infty x^{\frac{k}{2}}e^{-[(1+\rho)\beta_r - \frac{1}{8c^2}]x}I_0(2\sqrt{\rho}\beta_r x) [(\frac{x}{4c^2} + \frac{k}{2})D_{-k}(\sqrt{\frac{x}{2c^2}}) - \frac{\sqrt{x}}{\sqrt{8c^2}}D_{-k+1}(\sqrt{\frac{x}{2c^2}})]dx. \quad (14)$$

C. RIS in S-T Link

Similarly, if the S-T link uses RIS[1], h'_{st} is replaced by $\sum_{i=1}^{I}|p'_i||q'_i|$ in (5) to give

$$\rho \approx |1+\frac{\alpha\sigma_p\sigma_q\sigma_{tr}}{\sigma_{sr}}\frac{\sum_{i=1}^{I}|p'_i||q'_i|}{h'_{sr}}h'_{tr}|^2 \tag{15}$$

where p'_i is the normalized channel from the source to i-th element of RIS with $p'_i \sim \mathcal{CN}(0,1)$, q'_i is the normalized channel from the i-th element of RIS to the tag with $q'_i \sim \mathcal{CN}(0,1)$, σ_p^2 is the average fading power from source to RIS, σ_q^2 is the average fading power from RIS to tag, and other symbols are defined as before. Define $\beta_t = \frac{\sigma_{sr}^2}{\alpha^2\sigma_p^2\sigma_q^2\sigma_{tr}^2}$ and $X_t = \frac{|h'_{sr}|^2}{(\sum_{i=1}^{I}|p'_i||q'_i|)^2}$. Similarly, the CDF of X_t is derived as

$$F_{X_t}(x) = 1 - \frac{e^{\frac{1}{8c^2x}}}{(2c^2x)^{\frac{k}{2}}}D_{-k}(\frac{1}{\sqrt{2c^2x}}). \tag{16}$$

Then, the PDF of X_t can be derived by differentiating (16) and using it with the conditional PDF of ρ to give

$$f(\rho) = \frac{\beta_t}{(2c^2)^{\frac{k}{2}}}\int_0^\infty x^{-\frac{k}{2}}e^{\frac{1}{8c^2x}-(1+\rho)\beta_t x}I_0(2\sqrt{\rho}\beta_t x) \tag{17}$$
$$[(\frac{1}{4c^2x}+\frac{k}{2})D_{-k}(\frac{1}{\sqrt{2c^2x}}) - \frac{1}{\sqrt{8c^2x}}D_{-k+1}(\frac{1}{\sqrt{2c^2x}})]dx.$$

Compared with (14), one sees that x in (17) is inverse to x in (14), because X_t is inverse to X_r in distribution. Thus, the effect of k or I on the performance in this case is reverse to that in the previous subsection.

D. RIS in Both S-T and S-R Links

Finally, when both the S-R and S-T links use RIS, one has

$$\rho \approx |1+\frac{\alpha\sigma_p\sigma_q\sigma_{tr}}{\sigma_u\sigma_v}\frac{\sum_{i=1}^{I}|p'_i||q'_i|}{\sum_{i=1}^{I}|u'_i||v'_i|}h'_{tr}|^2. \tag{18}$$

Let $\beta_{rt} = \frac{\sigma_u^2\sigma_v^2}{\alpha^2\sigma_p^2\sigma_q^2\sigma_{tr}^2}$ and $X_{rt} = \frac{(\sum_{i=1}^{I}|u'_i||v'_i|)^2}{(\sum_{i=1}^{I}|p'_i||q'_i|)^2}$. Both $\sum_{i=1}^{I}|u'_i||v'_i|$ and $\sum_{i=1}^{I}|p'_i||q'_i|$ can be approximated as Gamma with shape parameter k and scale parameter c, as before. Their ratio follows a Beta prime distribution. Since X_{rt} is the square of Beta prime, its PDF is derived as

$$f_{X_{rt}}(x) = \frac{x^{\frac{k}{2}-1}}{2B(k,k)(1+\sqrt{x})^{2k}}, x>0 \tag{19}$$

where $B(\cdot,\cdot)$ is the Beta function [17, eq. (8.380.1)]. Thus, the unconditional PDF of ρ is

$$f(\rho) = \frac{\beta_{rt}}{2B(k,k)}\int_0^\infty \frac{(\sqrt{x})^k e^{-(1+\rho)\beta_{rt}x}}{(1+\sqrt{x})^{2k}}I_0(2\sqrt{\rho}\beta_{rt}x)dx. \tag{20}$$

Using (8), (14), (17) and (20) in (4), the average BER can be calculated. There are three key parameters: N, I and the DRR. From (3), the BER decreases when N increases. From (8), (14), (17) and (20), the PDF of ρ only depends on the DRR and k (or I), and it does not depend on individual values of σ_{st}^2, σ_{tr}^2 or σ_{sr}^2. From (8), (14), (17) and (20), the DDR appears as a scaling parameter. Thus, when β_o, β_r, β_t or β_{rt} increase, the PDF of ρ becomes more impulsive around 1 to increase the average BER. The value of k (or I) appears as a shaping parameter. A larger k leads to a mode of the PDF of ρ in (17) and (20) closer to 0 and that in (14) closer to 1 to reduce and increase the average BER, respectively, according to (3).

[1]From (5), h_{st} and h_{tr} are symmetric. Since the purpose of this letter is to examine the effect of RIS on individual links, we don't show the results for the case when the T-R link uses RIS. They can be easily obtained by replacing $\sigma_p\sigma_q\sigma_{tr}$ with $\sigma_p\sigma_q\sigma_{st}$ in the results in Section III.C. In the more general case when both the S-T and T-R links use RIS, it is expected that the performance will be "doubly" improved but its mathematical derivation seems not tractable.

IV. Numerical Results and Discussion

We set $\beta_o = \beta_r = \beta_t = \beta_{rt} = \beta$ for a fair comparison. Fig. 2 examines the accuracy of the large SNR and Gamma approximations. The definition of SNR follows the previous works on ambient backscatter communications [5], [6], and the values chosen are also similar to theirs. One sees from Fig. 2(a) that, when γ_s increases, the average BER approaches a lower limit. Thus, the large SNR approximations in Section III are accurate when γ_s is larger than 20 dB. To further see this, Fig. 2(b) compares simulation at $\gamma_s = 20dB$ with approximations in Section III. There is a perfect match, showing the accuracy of the approximations. In the following figures, we will only use the approximations derived in Section III.

From Fig. 3, when $I = 1$, the performance is better than when no RIS is used but as I increases, the performance degrades. Comparing (5) with (10), the only difference is that h'_{sr} in the denominator is replaced by the sum $\sum_{i=1}^{I}|u'_i||v'_i|$. When $I = 1$, $E\{\sum_{i=1}^{I}|u'_i||v'_i|\} = \frac{\pi}{4} < 1$. This increases ρ to reduce the BER. When $I \geq 2$, $E\{\sum_{i=1}^{I}|u'_i||v'_i|\} = I\frac{\pi}{4} > 1$. This reduces ρ to increase the BER. In general, the increase of the number of RIS elements in the S-R link is detrimental. From Fig. 4, when $I = 1$, the performance degrades but as I increases, the performance improves significantly. This is opposite to what observed from Fig. 3. Comparing (5) with (15), the only difference is that h'_{st} in the numerator is replaced by the sum $\sum_{i=1}^{I}|p'_i||q'_i|$. When $I = 1$, $E\{\sum_{i=1}^{I}|p'_i||q'_i|\} = \frac{\pi}{4} < 1$. This reduces ρ to increase the BER. However, when $I \geq 2$, $E\{\sum_{i=1}^{I}|p'_i||q'_i|\} = I\frac{\pi}{4} > 1$ This increases ρ to reduce the BER. Thus, increasing the number of RIS elements in the S-T link is beneficial. Fig. 5 uses RIS in both S-R and S-T links. As I increases, the BER performance improves. The improvement decreases with I.

V. Conclusion

The average BERs of ambient backscatter communications systems using RIS have been analyzed. The analysis uses the large SNR approximation as well as the Gamma approximation to obtain expressions in integral form rather than closed-form. Their accuracy has been examined. Numerical results have shown that an increase in the number of RIS elements in the S-R link degrades performance while an increase in the S-T link improves performance. This agrees with our intuition. However, our results quantify the performance change. What is not obvious is that, when both links use RIS, there is still performance improvement but it is marginal when the number of RIS elements increases. These conclusions are based on the

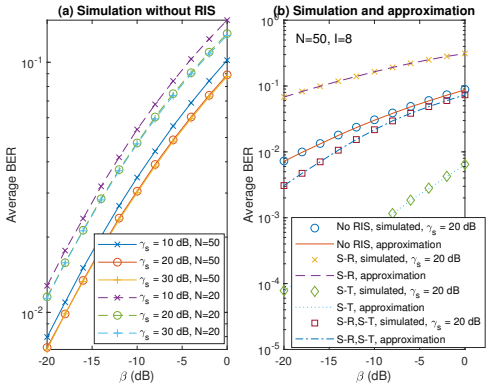

Fig. 2. Accuracy of approximation.

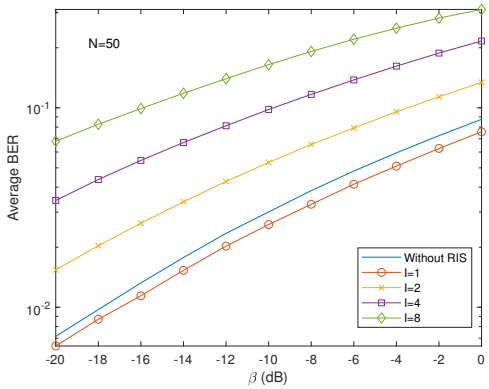

Fig. 3. Only the S-R link uses RIS (all curves are from approximations).

assumption that RIS is used to enhance the links, as often seen in the literature. On the other hand, RIS may also be used to weaken the links. For example, $\theta_i = \pi - \angle u_i - \angle v_i$ can be used to weaken the reflected signal in (9). This is equivalent to reducing the number of RIS elements. In this case, from our results, the S-R link should be weakened while the S-T or T-R links should be enhanced for better backscattering. Due to the limited space, this will be studied as a future work.

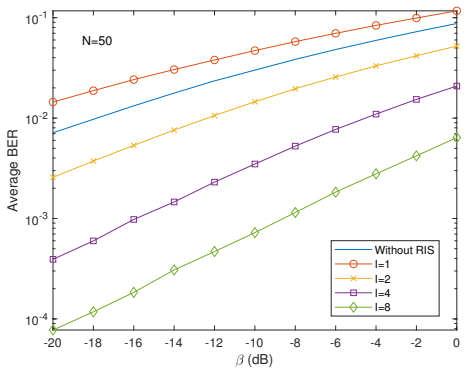

Fig. 4. Only the S-T link uses RIS (all curves are from approximations).

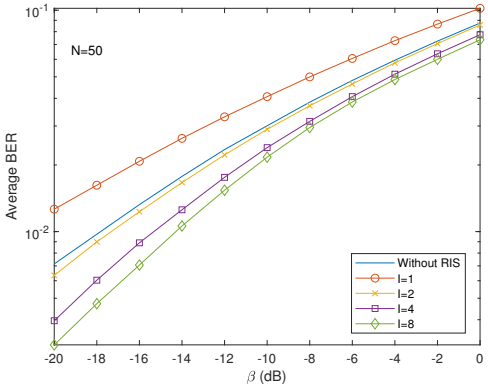

Fig. 5. Both the S-T and S-R links use RIS (all curves are from approximations).

REFERENCES

[1] A. Parks, A. Liu, S. Gollakota, and J. R. Smith, "Turbocharging ambient backscatter communication," *Proc. ACM SIGCOMM*, pp. 619 - 630, Chicago, IL, USA, Aug. 2014.

[2] B. Kellogg, A. Parks, S. Gollakota, J. R. Smith, and D. Wetherall, "Wi-Fi backscatter: Internet connectivity for RF-powered devices," *Proc. ACM SIGCOMM*, pp. 607 - 618, Chicago, IL, USA, Aug. 2014.

[3] B. Kellogg, V. Talla, S. Gollakota, and J. R. Smith, "Passive Wi-Fi: Bringing low power to Wi-Fi transmissions," *Proc. ACM SIGCOMM*, pp. 607 - 618, Chicago, IL, USA, Aug. 2014.

[4] D. Bharadia, K. R. Joshi, M. Kotaru, and S. Katti, "BackFi: high throughput WiFi backscatter," *Comput. Commun. Rev.*, vol. 45, pp. 283 - 296, Oct. 2015.

[5] J. Qian, F. Gao, G. Wang, S. Jin, H. Zhu, "Semi-coherent detection and performance analysis for ambient backscatter system," *IEEE Trans. Wireless Commun.*, vol. 65, pp. 5266 - 5278, Dec. 2017.

[6] Q. Tao, C. Zhong, H. Lin, Z. Zhang, "Symbol detection of ambient backscatter systems with Manchester coding," *IEEE Trans. Wireless Commun.*, vol. 17, pp. 4028 - 4038, June 2018.

[7] G. Yang, Y.-C. Liang, R. Zhang, Y. Pei, "Modulation in the air: backscatter communication over ambient OFDM carrier," *IEEE Trans. Commun.*, vol. 66, pp. 1219 - 1233, Mar. 2018.

[8] X. Li, M. Zhao, M. Zeng, et al, "Hardware impaired ambient backscatter NOMA systems: reliability and security," *IEEE Trans. Commun.*, vol. 69, pp. 2723 - 2736, Apr. 2021.

[9] G. Wang, F. Gao, R. Fan, C. Tellambura, "Ambient backscatter communication systems: detection and performance analysis," *IEEE Trans. Commun.*, vol. 64, pp. 1 - 10, Aug. 2016.

[10] M. Di Renzo, A. Zappone, M. Debbah et al., "Smart radio environments empowered by reconfigurable intelligent surfaces: how it works, state of research, and the road ahead," *IEEE Journal on Selected Areas in Communications*, vol. 38, pp. 2450 - 2525, Nov. 2020.

[11] E. Basar, M. Di Renzo, J. De Rosny, M. Debbah, M.-S. Alouini, R. Zhang, "Wireless communications through reconfigurable intelligent surfaces," *IEEE Access*, vol. 7, pp. 116753 - 116773, 2019.

[12] P. Xu, G. Chen, Z. Yang, M. Di Renzo, "Reconfigurable intelligent surfaces-assisted communications with discrete phase shifts: how many quantization levels are required to achieve full diversity?," *IEEE Wireless Commun. Lett.*, vol. 10, pp. 358 - 362, Feb. 2021.

[13] H. Zhang, B. Di, L. Song, et al, "Reconfigurable intelligent surfaces assisted communications with limited phase shifts: how many phase shifts are enough?," *IEEE Trans. Veh. Technol.*, vol. 69, pp. 4498 - 4502, Apr. 2020.

[14] M.-M. Zhao, Q. Wu, M.-J. Zhao, et al, "Exploiting amplitude control in intelligent reflecting surface aided wireless communication with imperfect CSI," *IEEE Trans. Commun.*, 2021.

[15] M. Nemati, J. Ding and J. Choi, "Short-range ambient backscatter communication using reconfigurable intelligent surfaces," *Proc. IEEE WCNC 2020*, Seoul, Korea, May 2020.

[16] X. Jia, X. Zhou, D. Niyato, and J. Zhao, "Intelligent reflecting surface-assisted bistatic backscatter networks: joint beamforming and reflection design," available at https://arxiv.org/abs/2010.08947.

[17] I.S. Gradshteyn, I.M. Ryzhik, *Tables of Integrals, Series and Products*, 6th Ed. Academic Press: London, 2000.

[18] J.G. Proakis, *Digital Communications*, 4th Ed. New York, NY: McGraw-Hill, 2001.